Behavioral/Cognitive

VPS26A–SNX27 Interaction-Dependent mGluR5 Recycling in Dorsal Horn Neurons Mediates Neuropathic Pain in Rats

Tzer-Bin Lin,[1,2,3] Cheng-Yuan Lai,[4,5]* Ming-Chun Hsieh,[4,6] Hsueh-Hsiao Wang,[4]* Jen-Kun Cheng,[4,7] Yat-Pang Chau,[4] Gin-Den Chen,[8] and Hsien-Yu Peng[4]

[1]Department of Physiology, School of Medicine, College of Medicine, Taipei Medical University, Taipei, Taiwan, [2]Graduate Institute of Basic Medical Science, College of Medicine, China Medical University, Taichung, Taiwan, [3]Department of Biotechnology, Asia University, Taichung, Taiwan, [4]Department of Medicine, Mackay Medical College, New Taipei, Taiwan, [5]Department of Veterinary Medicine, College of Veterinary Medicine, National Chung-Hsing University, Taichung, Taiwan, [6]Department of Physiology, College of Medicine, National Taiwan University, Taipei, Taiwan, [7]Department of Anesthesiology, Mackay Memorial Hospital, Taipei, Taiwan, and [8]Department of Obstetrics and Gynecology, Chung-Shan Medical University Hospital, Chung-Shan Medical University, Taichung, Taiwan

Retromer, which crucially contributes to endosomal sorting machinery through the retrieval and recycling of signaling receptors away from degradation, has been identified as a critical element for glutamatergic-receptor-dependent neural plasticity at excitatory synapses. We observed it accompanied by behavioral allodynia; neuropathic injury time-dependently enhanced VPS26A and SNX27 expression; VPS26A–SNX27 coprecipitation; and VPS26A-positive, SNX27-positive, and VPS26A–SNX27 double-labeled immunoreactivity in the dorsal horn of Sprague Dawley rats that were all sufficiently ameliorated through the focal knock-down of spinal VPS26A expression. Although the knock-down of spinal SNX27 expression exhibited similar effects, spinal nerve ligation (SNL)-enhanced VPS26A expression remained unaffected. Moreover, SNL also increased membrane-bound and total mGluR5 abundance, VPS26A-bound SNX27 and mGluR5 and mGluR5-bound VPS26A and SNX27 coprecipitation, and mGluR5-positive and VPS26A/SNX27/mGluR5 triple-labeled immunoreactivity in the dorsal horn, and these effects were all attenuated through the focal knock-down of spinal VPS26A and SNX27 expression. Although administration with MPEP adequately ameliorated SNL-associated allodynia, mGluR5 expression, and membrane insertion, SNL-enhanced VPS26A and SNX27 expression were unaffected. Together, these results suggested a role of spinal VPS26A–SNX27-dependent mGluR5 recycling in the development of neuropathic pain. This is the first study that links retromer-associated sorting machinery with the spinal plasticity underlying pain hypersensitivity and proposes the possible pathophysiological relevance of endocytic recycling in pain pathophysiology through the modification of glutamatergic mGluR5 recycling.

Key words: **retromer; SNX27; VPS26; mGluR5; neuropathic pain; allodynia**

Significance Statement

VPS26A–SNX27-dependent mGluR5 recycling plays a role in the development of neuropathic pain. The regulation of the VPS26A–SNX27 interaction that modifies mGluR5 trafficking and expression in the dorsal horn provides a novel therapeutic strategy for pain relief.

Introduction

Endocytic sorting of signaling receptors between recycling and degradative pathways is a key cellular process that controls the surface complement of receptors (Ehlers, 2000; Martin et al., 2004; Temkin et al., 2011). Retromer, a stable trimer composed of vacuolar protein sorting-associated protein 26 (VPS26), VPS29, and VPS35 (Collins et al., 2005; Hierro et al., 2007; Gallon et al., 2015), has been identified as a critical element of the endosomal sorting machinery that initiates cargo sorting for re-

Received July 8, 2015; revised Sept. 22, 2015; accepted Sept. 25, 2015.

Author contributions: H.-Y.P. designed research; T.-B.L., C.-Y.L., M.-C.H., H.-H.W., and H.-Y.P. performed research; C.-Y.L., M.-C.H., H.-H.W., J.-K.C., Y.-P.C., G.-D.C., and H.-Y.P. analyzed data; T.-B.L., M.-C.H., and H.-Y.P. wrote the paper.

This work was supported by the Ministry of Science and Technology, Taipei, Taiwan (Grants MOST 104-2320-B-715-004-MY3, NSC 102-2628-B-715-001, and 101-2320-B-715-001-MY3 to H.-Y.P. and Grants NSC MOST 104-2320-B-038-019-MY3, MOST 104-2320-B-038-027-MY3, 101-2320-B-039-013-MY3 to T.-B.L.), the Mackay Memorial Hospital (Grants MMH-MM-10206 and MMH-MM-10302 to H.-Y.P.), Taipei Medical University (Grant TMU102-AE1-B06 to T.-B.L.), and Saint Paul's Hospital (Grant SPMRD-U1-6003 to T.-B.L.).

The authors declare no competing financial interests.

*C.-Y.L. and H.-H.W. contributed equally to this work.

Correspondence should be addressed to Hsien-Yu Peng, Department of Medicine, Mackay Medical College, No.46, Sec. 3, Zhongzheng Rd, Sanzhi Dist, New Taipei, Taiwan 25245. E-mail: hsien.yu@gmail.com.

DOI:10.1523/JNEUROSCI.2587-15.2015

 0270-6474/15/3514943-13$15.00/0

trieval and recycling to the plasma membrane or *trans*-Golgi network and therefore away from degradation (Cullen et al., 2011). Mammalian-retromer-dependent recycling of the signaling receptor is associated with glutamatergic receptor-dependent neural plasticity at excitatory synapses in multiple neuropathologies, such as Alzheimer's disease (Wen et al., 2011) and Down's syndrome (Wang et al., 2013). However, the potential contribution of retromer-dependent cycling in spinal glutamate-receptor-associated pain hypersensitivity has not been established.

Sorting nexin (SNX)27, an endosome-associated cargo adaptor, is unique among SNXs because this protein possesses a PDZ domain (Wang et al., 2013; Gallon et al., 2014). The direct interaction of the PDZ domain of SNX27 with the retromer subunit VPS26A is necessary for the recognition and recycling of PDZ motif-containing cargo (Steinberg et al., 2013; Gallon et al., 2014) from the endosome toward the plasma membrane (Temkin et al., 2011; Gallon and Cullen, 2015). Notably, through a PDZ-dependent mechanism, SNX27 promotes the recycling and membrane insertion of the glutamatergic receptor (Wang et al., 2013), a key player in pain-associated neural plasticity (Larsson et al., 2011; Peng et al., 2013; Luo et al., 2014). Therefore, the SNX27-VPS26A complex is emerging as a potential link between glutamatergic receptor recycling and the spinal mechanism underlying neuropathic pain development.

Metabotropic glutamate receptor 5 (mGluR5) undergoes cargo cycling in HEK293 cells (Trivedi et al., 2012). Inflammatory pain increases the abundance and membrane insertion of mGluR5 in the dorsal horn (Pitcher et al., 2007). However, the potential contribution of cargo cycling in pain-enhanced mGluR5 abundance/trafficking remains unclear. Moreover, although the role of the SNX27–retromer complex in the endosomal recycling of mGluR5 has not been established, considering that SNX27 contributes to the subcellular recycling of G-protein-coupled receptor (GPCR) through the PDZ-mediated protein-protein interactions (Magalhaes et al., 2012; Bauch et al., 2014; Dunn et al., 2015) and the fact that mGluR5 is characterized by a GPCR that contains a PDZ-binding motif (Kitano et al., 2002), we hypothesized that the VPS26A–SNX27 complex participates in neuropathic pain development through the modification of endosomal sorting-associated membrane trafficking and the degradation of mGluR5 in dorsal horn neurons.

Materials and Methods

Animal preparations. Adult male Sprague Dawley rats weighing 200–250 g were used throughout this study. All animal procedures in this study were conducted in accordance with the guidelines of the International Association for the Study of Pain (Zimmermann, 1983) and were reviewed and approved by the Institutional Review Board of Taipei Medical University, Taipei, Taiwan.

Spinal nerve ligation. Spinal nerve ligation rat model was performed as described by previous studies (Lin et al., 2015a,b). Briefly, the rats were anesthetized under isoflurane anesthesia (induction 5%, maintenance 2% in air). An incision was made and the left L5–L6 spinal nerves were carefully were dissected and tightly ligated with 6-0 silk sutures 2–5 mm distal to the dorsal root ganglia. In the sham operation group, the surgical procedures were identical to the nerve ligation group except the silk sutures were left unligated.

Intrathecal catheter. Implantation of intrathecal cannulae was performed as described in our previous study (Peng et al., 2013). Briefly, PE-10 SILASTIC tubing was implanted in the lumbar enlargement of the spinal cord. The outer part of the catheter was plugged and immobilized onto the skin on closure of the wound. After implantation, the animals were allowed to recover for 3 d and were then used for behavioral tests, Western blotting, coprecipitation, or immunohistochemistry. Rats showing neurological deficits after surgery were killed and excluded from statistical analyses.

Behavioral studies. Tactile sensitivity was assessed by measuring each rat's paw-withdrawal threshold in response to probing with von Frey monofilaments (Stoelting) according to the method of Schäfers et al. (2003). In brief, rats were placed individually in an opaque plastic cylinder, which was placed on a wire mesh. Animals were habituated for 1 h to allow acclimatization to the test environment before each test. After acclimatization, calibrated von Frey filaments (0.07–26.0 g) were applied to the plantar surfaces of the hindpaws of rats. The withdrawal threshold was assayed 1 d before surgery to ensure that the animals had normal tactile sensitivity. Because a previous study showed that the mean withdrawal threshold of naive rats was ~15 g (Kim and Chung, 1992), rats that displayed a threshold lower or higher than 15 g were excluded from further study. Motor function was assessed using an accelerating Rotarod apparatus (LE8500; Ugo Basile). For acclimatization, the animals were subjected to three training trials at 3–4 h intervals on 2 separate days. During the training sessions, the rod was set to accelerate from 3 to 30 rpm over a 180 s period. During the test session, the performance times of rats were recorded up to a cutoff time of 180 s. Three measurements were obtained at intervals of 5 min and were averaged for each test.

Western blotting. In brief, the dissected dorsal horn (L4–L5) sample was homogenized in 25 mM Tris-HCl, 150 mM NaCl, 1% NP-40, 1% sodium deoxycholate, and 0.1% SDS with a complete protease inhibitor mixture (Roche). After incubation on ice (1 h), the lysates were centrifuged (14,000 rpm, 20 min, 4°C). All of the protein concentrations were determined using a bicinchoninic acid assay. The supernatant was separated on an acrylamide gel and transferred to a polyvinylidene difluoride membrane, which was then incubated (1 h, room temperature) in either rabbit anti-SNX27 (SNX27, 1:1000; Santa Cruz Biotechnology, Santa Cruz, CA), rabbit anti-VPS26A (1:1000; Abcam, Cambridge), rabbit anti-mGluR5 (1:4000; Abcam, Cambridge), or mouse anti-Glyceraldehyde 3-phosphate dehydrogenase (GAPDH, 1:4000; Santa Cruz Biotechnology, Santa Cruz, CA). The blots were washed and incubated (1 h, room temperature) in peroxidase-conjugated goat anti-rabbit IgG (1:8000; Jackson ImmunoResearch), goat anti-mouse IgG (1:8000; Jackson ImmunoResearch) or rabbit anti-sheep IgG (1:8000; Millipore, Billerica, Massachusetts). The protein bands were visualized using an enhanced chemiluminescence detection kit (ECL Plus; Millipore) and then subjected to a densitometric analysis with Science Lab 2003 (Fuji).

Preparation of spinal synaptosomal membrane fractionation. In experiments assaying the amount of synaptosomal membrane-bound protein in spinal cord, we used methods adapted from studies (Galan et al., 2004; Hallett et al., 2008; Peng et al., 2012). In brief, the dissected dorsal horn (L4–L5) samples were homogenized and centrifuged (7500 rpm, 5 min). The supernatant containing cytosol (S1) was separated from the pellet containing nuclei plus debris (P1). The collected supernatant was then centrifuged (13,000 rpm, 1 h) again to obtain pure cytosol from the supernatant (S2) and crude synaptosomal membrane from the pellet (P2). The crude synaptosomal membrane was resuspended in PBS. Protein amounts were finally measured and prepared for Western blotting as explained above. The amount of synaptosomal membrane-bound mGluR5 in spinal cord was measured by assaying the abundance of mGluR5 in the membrane fraction (P2) using an antibody identical to that used to measure the total mGluR5 (rabbit, 1:4000; Abcam) in the total spinal tissue.

Coprecipitation. Rabbit polyclonal antibody against VPS26A, SNX27 or mGluR5 was incubated (overnight, 4°C) with the dorsal horn extracts. The 1:1 slurry protein agarose suspension (Millipore) was added into this protein immunocomplex and the mixture was incubated for 2–3 h at 4°C. The agarose beads were washed once with 1% (v/v) Triton X-100 in an immunoprecipitation buffer (50 mM Tris-Cl, pH 7.4, 5 mM EDTA, 0.02% (w/v) sodium azide), twice with 1% (v/v) Triton X-100 in an immunoprecipitation buffer containing 300 mM NaCl, and thrice with an immunoprecipitation buffer only. The bound proteins were eluted with SDS PAGE sample buffer at 95°C. The proteins were separated by SDS PAGE, electrophoretically transferred to polyvinylidene difluoride membranes, and detected using rabbit anti-SNX27 (1:1000; Santa Cruz

Biotechnology), rabbit anti-VPS26A (1:1000; Abcam), and rabbit anti-mGluR5 (1:4000; Abcam).

Immunofluorescence. After perfusion (100 ml of PBS followed by 300 ml of paraformaldehyde; 4%; pH7.4), the spinal cord samples were harvested (L4–L5), postfixed (4°C for 4 h), and cryoprotected in sucrose solution (30%) overnight. The samples were double labeled to investigate interactions between SNX27 and neuronal/glial/microglia markers; specifically, the spinal sections were incubated overnight (4°C) with a mixture of rabbit anti-SNX27 (1:200; Santa Cruz Biotechnology) and mouse monoclonal anti-neuronal nuclear antigen (NeuN, a neuronal marker, 1:500; Millipore), mouse anti-glial fibrillary acidic protein (a marker of astroglial cells; 1:1000; Millipore), or mouse anti-integrin αM (OX-42, a marker of microglia; 1:500; Santa Cruz Biotechnology). After rinsing in PBS three times, the sections were then incubated (1 h, 37°C) with Alexa Fluor 488 (1:1500; Invitrogen) and Alexa Fluor 594 (1:1500; Invitrogen). When examining the interaction among SNX27, VPS26, and mGluR5, the specific antibodies were mixed with 10× reaction buffer (Mix-n-Stain; Biotium) with the antibody solution at a ratio of 1:10. Then, the solution was transferred to the virus-containing dye (CF; Biotium) and incubated in the dark (30 min, room temperature). The spinal cord sections were sequentially incubated (overnight, 4°C) with dilute solutions: rabbit anti-SNX27 (1:200; Santa Cruz Biotechnology), rabbit anti-VPS26A (1:200; Abcam), and rabbit anti-mGluR5 (1:200; Abcam) and washed 5 times between each incubation. Spinal sections were subsequently rinsed in PBS and coverslips were applied. When these fluorescent markers are excited, they can be easily detected by a charge coupled device (X-plorer; Diagnostic Instruments) through a fluorescent microscopy (DM2500; Leica). Five spinal cord sections in each rat were used for cell counting. Cell counting was performed under a microscope at the magnification of 200×.

Small-interfering RNA. The 19-nucleotide duplexes of the small-interfering RNAs (siRNAs) for SNX27 were 5′-GUACUUCUUUCA UCAGGCU-3′. The 19-nucleotide duplexes of the small-interfering RNAs (siRNAs) for VPS26A were 5′-CUAUUCCGAUAAGAUUGUU-3′. The missense or siRNA was intrathecally administered with a polyethyleneimine (10 μl, Al 25 kDa; Sigma-Aldrich)-based gene-delivery system into the dorsal subarachnoid space (L4–L5) of animals through the implanted catheter (daily for 4 d from day 3–6 after spinal nerve ligation, SNL).

Drug application. MPEP (a mGluR5 antagonist; 10, 100, and 300 nM; 10 μl Tocris Bioscience; bolus at day 7 or daily from day 3 to 6 after SNL; intrathecal) were administered intrathecally via a bolus injection. A vehicle solution of a volume identical to that of the tested agents was dispensed to serve as a control.

Data analysis. All of the data in this study were analyzed using SigmaPlot version 10.0 (Systat Software) or Prism 6.0 (GraphPad) and are expressed as the mean ± SEM. Paired two-tailed Student's *t* test was used to compare the means between groups. One-way or two-way ANOVAs were used to assess changes in values for serial measurements over time and *post hoc* Tukey's tests were used to compare the means of groups. Significance was set at $p < 0.05$.

Results

Nerve ligation induces allodynia associated with spinal SNX27 expression

We first investigated whether spinal SNX27 plays a role in the development of neuropathic pain. Western blots revealed that SNL significantly increased the abundance of SNX27 in the ipsilateral, but not the contralateral, dorsal horn at days 3, 7, 14, and 21 after operation (Fig. 1*A*). In contrast, the sham operation did not alter SNX27 expression in the ipsilateral or the contralateral dorsal horn. To visualize the cellular location of SNL-induced SNX27 expression, spinal slices were stained with the specific antibody at day 7 after operation, when the animals displayed maximal allodynia and spinal SNX27 expression. As anticipated, SNL increased SNX27 immunofluorescence in the ipsilateral dorsal horn, and double-labeled staining revealed that SNX27 immunofluorescence colocalized with neuronal, but not microglial or astrocyte markers (Fig. 1*B*), indicating that SNL specifically upregulates SNX27 expression in the ipsilateral dorsal horn neurons. Moreover, consistent with the time profile of SNX27 expression, we observed that SNL significantly decreased the withdrawal latency of the ipsilateral hindpaw at days 3, 7, 14, and 21 after operation (Fig. 1*C*). These results suggested that neuropathic injury induces nociception hypersensitivity associated with enhanced SNX27 expression in the ipsilateral dorsal horn neurons.

Knock-down of spinal SNX27 expression ameliorates SNL-induced allodynia

To provide further evidence supporting the role of spinal SNX27 in the development of neuropathic pain, we generated rats in which spinal SNX27 expression was knocked down focally through daily intrathecal administration with specific antisense siRNA. Western blot analyses demonstrated that the abundance of SNX27 in dorsal horn samples was dose-dependently decreased through intrathecal injection with SNX27 mRNA-targeting siRNA (1, 2, and 3 μg, 10 μl, once daily for 4 d; Fig. 2*A*), but not with missense siRNA (3 μg, 10 μl), polyethylenimine (a transfection reagent, 10 μl), or intrathecal catheter implantation alone, indicating that spinal SNX27 expression was sufficiently knocked down by specific siRNAs. Subsequent analyses using Rotarod tests to evaluate the motor performance of rodents showed that there was no significant difference between the naive and polyethylenimine-missense siRNA (3 μg, 10 μl)- or SNX27 mRNA-targeting siRNA (3 μg, 10 μl)-treated groups (Fig. 2*B*), suggesting that neither of these procedures nor spinal SNX27 knock-down led to motor deficits in these animals. The results of the von Frey test showed no effect on the withdrawal threshold of sham-operated animals (Fig. 2*C*), whereas treatment with SNX27 mRNA-targeting siRNA (3 μg, 10 μl), as anticipated, partially ameliorated SNL-induced behavioral allodynia, as evidenced by a significant increase of the withdrawal threshold at days 5 and 7 after operation (Fig. 2*D*). Moreover, SNX27 mRNA-targeting siRNA (3 μg, 10 μl) significantly decreased SNL-enhanced SNX27 expression in the ipsilateral dorsal horn at day 7 after operation (Fig. 2*E*). Collectively, the data obtained from the knock-down rats suggested that spinal SNX27 notably contributed to SNL-associated pain hypersensitivity.

SNL enhances VPS26A–SNX27 coupling in the dorsal horn

Crystal structure analysis has demonstrated that VPS26A, a retromer subunit, binds to the PDZ domain of SNX27 (Gallon et al., 2014), revealing that VPS26A and SNX27 work cooperatively. We thereby hypothesized that spinal SNX27 participates in neuropathic pain through the formation of the VPS26A–SNX27 complex. To further test this hypothesis, we first examined the VPS26A–SNX27 interaction after SNL using immunoprecipitation analysis. As anticipated, SNL enhanced the abundance of SNX27-bound SNX27, SNX27-bound VPS26A, VPS26A-bound VPS26A, and VPS26A-bound SNX27 coprecipitates in the ipsilateral dorsal horn on day 7 after operation compared with the sham operation, indicating that SNX27 did coprecipitate with VPS26A in the SNL dorsal horn on day 7 (Fig. 3*A*). We next assessed the expression profiles of VPS26A in the dorsal horn in response to SNL using Western blot analysis. Interestingly, SNL also significantly increased the abundance of VPS26A specifically in the ipsilateral dorsal horn on days 3, 7, 14, and 21 after the operation (Fig. 3*B*). We then examined the location of the VPS26A–SNX27 interactions using immunohistochemistry and

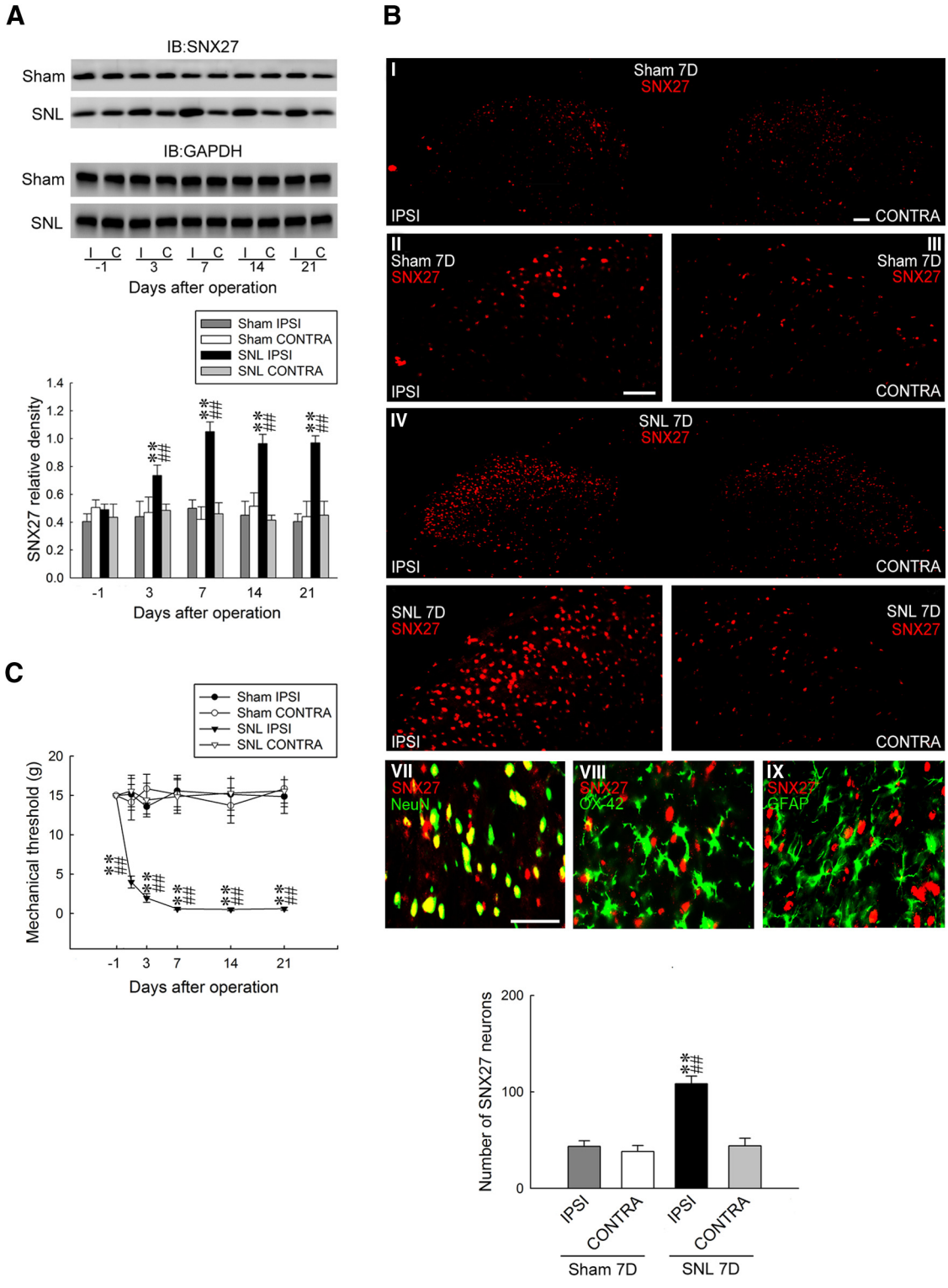

Figure 1. Nerve ligation upregulates SNX27 expression in dorsal horn neurons accompanied with allodynia. ***A***, Representative Western blot and statistical analyses (normalized to GAPDH) revealing that SNL, but not the sham operation (sham), increased SNX27 expression at days 3, 7, 14, and 21 after operation specifically in the ipsilateral (I and IPSI), but not the contralateral (C and CONTRA), dorsal horn. Two-way ANOVA with repeated measures over time, group ($F_{(3,20)} = 35.7$; $p < 0.001$), and time ($F_{(4,80)} = 2.465$; $p = 0.051$) and in the interaction of group by time ($F_{(12,80)} = 2.650$; $p = 0.004$), *post hoc* Tukey's tests. $^{**}p < 0.01$ vs sham IPSI. $^{\#\#}p < 0.01$ vs SNL day −1. $n = 6$. IB, Immunoblotting. ***B***, At day 7 after the operation, SNL increased the SNX27 immunofluorescence (red) in the ipsilateral dorsal horn (SNL 7D) that was colocalized with the immunoreactivity of neuronal (NeuN, green, VII), but rather than microglial (OX-42, green, VIII) or astrocyte (GFAP, green, IX) markers. Paired two-tailed Student's *t* test, $^{**}p < 0.01$ vs sham IPSI. $^{\#\#}p < 0.01$ vs SNL CONTRA. $n = 7$. Scale bar, 50 μm. Thickness, 50 μm. ***C***, The withdrawal threshold of the ipsilateral, but not the contralateral, hindpaw was decreased at days 1, 3, 7, 14, and 21 after SNL (von Frey test). Two-way ANOVA with repeated measures over time, group ($F_{(3,24)} = 54{,}09$; $p < 0.001$), and time ($F_{(5,120)} = 3.185$; $p = 0.009$) and in the interaction of group by time ($F_{(15,120)} = 3.324$; $p < 0.001$), *post hoc* Tukey's tests. $^{**}p < 0.01$ vs sham IPSI; $^{\#\#}p < 0.01$ vs SNL day −1. $n = 7$.

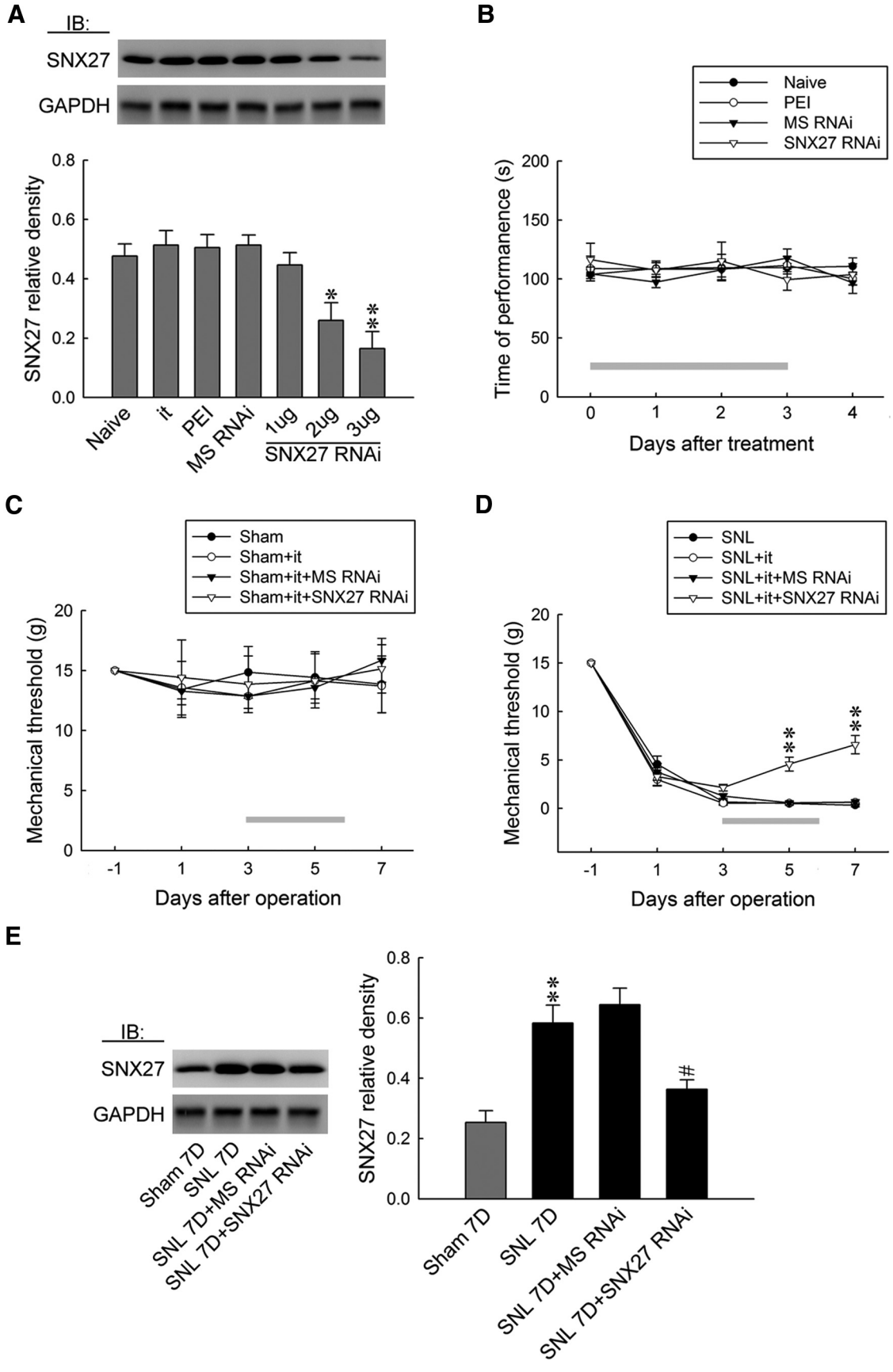

Figure 2. Focal knock-down of spinal SNX27 expression relieves SNL-induced allodynia. ***A***, Representative Western blot and statistical analyses (normalized to GAPDH) demonstrating intrathecal administration with SNX27 mRNA-targeting siRNA (SNX27 RNAi; 1, 2, and 3 μg; 10 μl), but not missense siRNA (MS RNAi, 3 μg, 10 μl), polyethylenimine (PEI, 10 μl), or intrathecal catheter implantation alone (it), dose-dependently decreased spinal SNX27 expression. One-way ANOVA, $F_{(6,35)} = 8.8886$, $p < 0.001$, *post hoc* Tukey's tests. (*Figure legend continues.*)

observed that SNL, but not the sham operation, notably enhanced VPS26A, SNX27, and VPS26A/SNX27 double-labeled immunoreactivity in the ipsilateral dorsal horn at 7 d after the operation (Fig. 3*C*). Based on these results, we further investigated the involvement of VPS26–SNX27 interactions in the induction and maintenance of neuropathic pain using coprecipitation analysis. The dorsal horn samples were obtained on days 3 and 7 after surgery, reflecting the induction (Wang et al., 2011) and maintenance (Lee et al., 2011) phases of neuropathic pain, respectively. Coprecipitation analysis demonstrated that SNL notably increased the amounts of VPS26A-bound VPS26A and VPS26A-bound SNX27 at days 3 and 7 after SNL and, reciprocally, SNL also increased the abundance of SNX27-bound SNX27 and SNX27-bound VPS26A at the identical time points (Fig. 3*D*). These results suggested that, in association with SNX27, SNL upregulated spinal VPS26A expression and enhanced VPS26A–SNX27 coupling in the dorsal horn.

Knock-down of spinal VPS26A expression attenuates SNL-induced allodynia and SNX27 expression

To further confirm the role of VPS26A in neuropathic pain development, we examined whether the lack of spinal VPS26A affects SNL-induced allodynia. Western blot analyses demonstrated that the spinal application of VPS26A mRNA-targeting siRNA (1, 3, and 5 μg, 10 μl, once daily for 4 d), but not missense siRNA (5 μg, 10 μl), polyethylenimine (10 μl), or an intrathecal catheter implantation alone dose-dependently decreased the abundance of VPS26A in the dorsal horn (Fig. 4*A*), indicating that antisense siRNA sufficiently knocked down spinal VPS26A expression. Moreover, neither the procedure itself nor the knock-down of spinal VPS26A resulted in motor deficits in animals (Fig. 4*B*). The results of the von Frey test demonstrated that, although no effect on the withdrawal threshold of sham-operated animals was observed (Fig. 4*C*), administration with VPS26A mRNA-targeting siRNA (5 μg, 10 μl), as anticipated, partially ameliorated SNL-induced behavioral allodynia by significantly increasing the withdrawal threshold at days 5 and 7 after the operation (Fig. 4*D*). Notably, although the knock-down of spinal VPS26A expression (5 μg, 10 μl) significantly decreased both SNL-enhanced VPS26A and SNX27 expression at day 7 after the operation, the administration of SNX27 mRNA-targeted antisense siRNA (3 μg, 10 μl) did not reduce the SNL-enhanced abundance of VPS26A despite the fact that the abundance of SNX27 was significantly decreased in the ipsilateral dorsal horn (Fig. 4*E*). These results suggest that VPS26A crucially contributes to the development of neuropathic pain through its association with and regulation of downstream spinal SNX27.

SNL-induced VPS26A–SNX27 coupling is accompanied by enhanced spinal mGluR5 expression

The direct PDZ interaction between VPS26 and SNX27 was demonstrated as necessary and sufficient to prevent the lysosomal entry of SNX27 cargo (Steinberg et al., 2013). The SNX27–retromer complex was implicated in the regulation of glutamatergic receptors (Wang et al., 2013) and GPCR (Bauch et al., 2014) through binding to the PDZ motif (Loo et al., 2014; Wang et al., 2013; Gallon et al., 2014). Considering that glutamatergic mGluR5, which is crucial for pain-associated spinal plasticity (Pitcher et al., 2007), is a GPCR containing PDZ motif (Kitano et al., 2002), we hypothesized that the VPS26A–SNX27 complex contributes to neuropathic pain through the modification of the endosomal recycling of spinal mGluR5, which prevents mGluR5 from degradation. To examine this hypothesis, we first assessed whether SNL affects spinal mGluR5 expression. Western blot analysis demonstrated that SNL increased mGluR5 abundance specifically in the ipsilateral dorsal horn samples on days 3 and 7 after operation (Fig. 5*A*). Conversely, on day 7 after SNL, bolus injections of MPEP (an mGluR5 antagonist; 10, 100, and 300 nM, 10 μl, i.t.) dose-dependently ameliorated SNL-induced allodynia, as evidenced by a significant increase of the withdrawal threshold of the ipsilateral hindpaw at hours 2, 3, 4, 5, and 6 after injection (Fig. 5*B*). There was no affect in the contralateral hindpaw at 3 h after injection, the time point at which MPEP exhibited maximal anti-allodynic effects on the ipsilateral side. These results suggested that spinal mGluR5 crucially contributes to SNL-induced allodynia.

Further analyses showed that daily spinal administration (for 4 d from day 3–6 after SNL) with VPS26A mRNA-targeting siRNA (5 μg, 10 μl), SNX27 mRNA-targeting siRNA (3 μg, 10 μl), and MPEP (100 nM, 10 μl) ameliorated the SNL-enhanced abundance of spinal mGluR5 on day 7 after operation (Fig. 5*C*). In contrast, the daily injection of MPEP (100 nM, 10 μl) did not affect SNL-enhanced spinal VPS26A or SNX27 expression (Fig. 5*D*). In addition, immunohistochemical analyses revealed that SNL, but not the sham operation, enhanced SNX27, VPS26A, mGluR5, and SNX27/VPS26A/mGluR5 triple-labeled immunoreactivity in the ipsilateral dorsal horn on day 7 after the operation (Fig. 5*E*). Daily spinal administration with MPEP (100 nM, 10 μl) ameliorated the SNL-enhanced mGluR5-labeled immunoreactivity in the ipsilateral dorsal horn on day 7 after the operation, but it did not affect SNL-enhanced spinal VPS26A or SNX27 expression. Furthermore, the immunoprecipitation of VPS26A and mGluR5 from the ipsilateral dorsal horn samples dissected on day 7 after the operation showed that SNL increased the abundance of VPS26A-bound VPS26A, SNX27, and mGluR5; SNL also increased the abundance of mGluR5-bound mGluR5, VPS26A, and SNX27 and these effects were all attenuated by daily administration of VPS26A mRNA-targeting siRNA (5 μg, 10 μl; Fig. 5*F*). Although the application of SNX27 mRNA-targeting siRNA (3 μg, 10 μl) elicited similar effects as VPS26A mRNA-specific antisense siRNA (5 μg, 10 μl), SNL-enhanced VPS26A-bound VPS26 expression in the precipitates was not reduced. Moreover, daily spinal administration of MPEP (100 nM, 10 μl) ameliorated the SNL-enhanced VPS26A-bound mGluR5, mGluR5-bound mGluR5, mGluR5-bound VPS26A, and mGluR5-bound SNX27 in the ipsilateral dorsal horn at day 7 after the operation, but did not affect the SNL-enhanced spinal VPS26A-bound VPS26A and VPS26A-bound SNX27

←

(*Figure legend continued.*) $^{*}p < 0.05$, $^{**}p < 0.01$ vs Naive. $n = 6$. IB, Immunoblotting. ***B***, The application of SNX27 mRNA-targeting siRNA (3 μg, 10 μl) resulted in no motor deficits in animal (Rotarod test). Two-way ANOVA with repeated measures over time, group ($F_{(3,24)} = 0.298$; $p = 0.826$) and time ($F_{(4,96)} = 0.495$; $p = 0.738$), and in the interaction of group by time ($F_{(12,96)} = 0.504$; $p = 0.907$), *post hoc* Tukey's tests. $n = 7$. ***C***, ***D***, Although no effect on the withdrawal threshold of sham-operated animals was observed, focal knock-down of spinal SNX27 expression (SNL+it+SNX27 RNAi, 3 μg, 10 μl) ameliorated the SNL-decreased withdrawal threshold at days 5 and 7 after the operation (von Frey test). sham group: Two-way ANOVA with repeated measures over time, group ($F_{(3,24)} = 0.112$; $p = 0.952$) and time ($F_{(4,96)} = 0.479$; $p = 0.750$) and in the interaction of group by time ($F_{(12,96)} = 0.161$; $p = 0.999$), *post hoc* Tukey's tests. $n = 7$. SNL group: Two-way ANOVA with repeated measures over time, group ($F_{(3,24)} = 15.83$; $p < 0.001$) and time ($F_{(4,96)} = 701.1$; $p < 0.001$) and in the interaction of group by time ($F_{(12,96)} = 10.46$; $p < 0.001$), *post hoc* Tukey's tests. $^{**}p < 0.01$ vs SNL. $n = 7$. ***E***, The SNL-enhanced spinal SNX27 expression at day 7 after the operation was attenuated through the administration of SNX27 mRNA-targeting siRNA (SNL+it+SNX27 RNAi, 3 μg, 10 μl). One-way ANOVA, $F_{(3,20)} = 14.91$, $p < 0.001$, *post hoc* Tukey's tests. $^{**}p < 0.01$ vs sham 7D. $^{\#}p < 0.05$ vs SNL7D. $n = 6$.

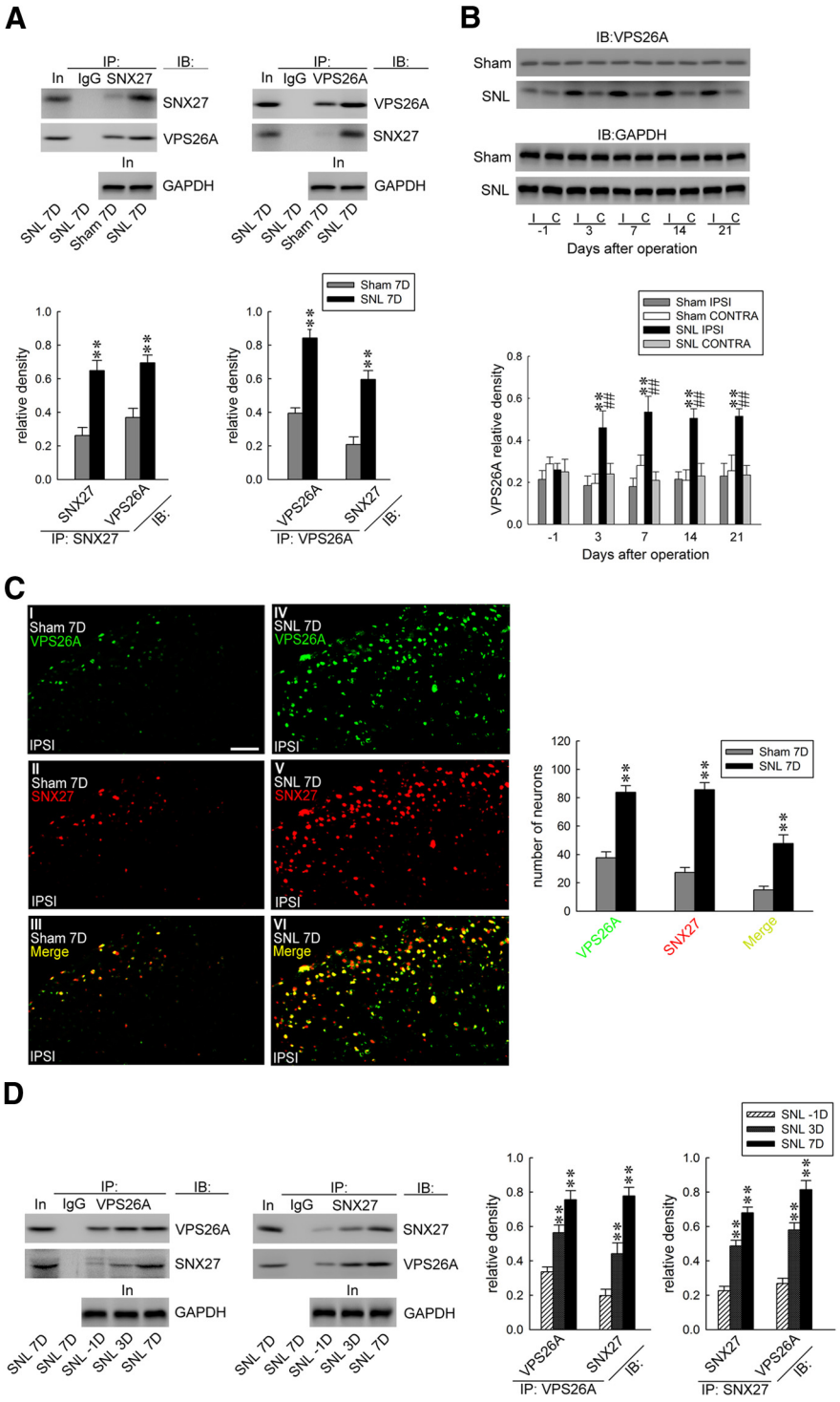

Figure 3. SNL enhances VPS26A–SNX27 coupling and VPS26A expression in the dorsal horn. ***A***, At day 7 after SNL, SNX27 coprecipitates with VPS26A in ipsilateral dorsal horn samples (SNL 7D). Paired two-tailed Student's *t* test, $^{**}p < 0.01$ vs sham 7D. $n = 6$. No detectable immunoreactivity was observed in the control IgG precipitation. IB, immunoblotting; In, input control; IP, immunoprecipitation. ***B***, Representative Western blot and statistical analyses (normalized to GAPDH) revealing that SNL, but not the sham operation (sham), increased VPS26A expression at days 3, 7, 14, and 21 after operation selectively in the ipsilateral (I and IPSI), but not the contralateral (C and CONTRA), dorsal horn. Two-way ANOVA with repeated measures over time, group ($F_{(3,20)} = 37.91; p < 0.001$) and time ($F_{(4,80)} = 1.702; p = 0.157$) and in the interaction of group by time ($F_{(12,80)} = 2.367; p = 0.011$), *post hoc* Tukey's tests. $^{**}p < 0.01$ vs sham IPSI. $^{\#\#}p < 0.01$ vs SNL day −1. $n = 6$. ***C***, Images demonstrating SNL increased VPS26A (green), SNX27 (red), and SNX27/VPS26A double-labeled (yellow) immunofluorescence in the ipsilateral dorsal horn at day 7 after the operation (SNL 7D). Paired two-tailed Student's *t* test, $^{**}p < 0.01$ vs sham 7D. $n = 7$. Scale bar, 50 μm. Thickness, 50 μm. ***D***, Reciprocal immunoprecipitation analysis showing that SNL enhanced the abundance of VPS26A-bound VPS26A and SNX27 (IP: VPS26A) and SNX27-bound SNX27 and VPS26A (IP:SNX27) in the ipsilateral dorsal horn samples at days 3 and 7 after the operation. The abundance of GAPDH in the preprecipitated homogenates obtained at these time points remained at a relative constant level.

interaction. These data suggested that the SNL-enhanced spinal VPS26A–SNX27 complex binds to mGluR5 and subsequently increases the amount of mGluR5 underlying neuropathic pain.

VPS26A–SNX27-complex drives mGluR5 membrane trafficking to mediate neuropathic pain

Previous studies have demonstrated that the VPS26A–SNX27 complex recycles PDZ motif-containing cargo (Steinberg et al., 2013; Gallon et al., 2014) from the endosome toward the plasma membrane (Temkin et al., 2011; Gallon and Cullen, 2015) through direct binding to their PDZ motifs (Loo et al., 2014; Wang et al., 2013). Therefore, we next analyzed whether the spinal VPS26A–SNX27 complex also regulates spinal mGluR5 recycling through the modification of subcellular mGluR5 redistribution to underlie the observed SNL-induced allodynia. Western blot analysis demonstrated that SNL significantly increased the abundance of synaptosomal membrane-bound mGluR5 [mGluR5(m)] (Fig. 6*A*), specifically in the ipsilateral dorsal horn at days 3 and 7 after operation. At day 7 after the operation, the focal knock-down of spinal VPS26A expression (5 μg, 10 μl), focal knock-down of spinal SNX27 expression (3 μg, 10 μl), and daily application of MPEPs (300 nM, 10 μl) all ameliorated the SNL-enhanced abundance of synaptosomal membrane-bound mGluR5 in the dorsal horn (Fig. 6*B*). Together with these data, these findings suggest that the VPS26A–SNX27 complex interacts with mGluR5 and thereby facilitates mGluR5 membrane trafficking in dorsal horn neurons, underlying the behavioral allodynia induced through neuropathic injury.

Discussion

In the present study, we demonstrated that an experimental neuropathic injury upregulates the abundance of spinal VPS26A and SNX27 and that VPS26A recruits and interacts with SNX27. The SNL-induced VPS26A–SNX27 complex subsequently interacts with mGluR5 to promote mGluR5 recycling, thereby enhancing the amount of total and membrane-bound mGluR5 in dorsal

←

VPS26A-bound VPS26A, one-way ANOVA, $F_{(2,15)} = 24.08$, $p < 0.001$; VPS26A-bound SNX27, one-way ANOVA, $F_{(2,15)} = 32.87$, $p < 0.001$; SNX27-bound SNX27, one-way ANOVA, $F_{(2,15)} = 54.75$, $p < 0.001$; SNX27-bound VPS26A, one-way ANOVA, $F_{(2,15)} = 42.24$, $p < 0.001$. All *post hoc* Tukey's tests, $^{**}p < 0.01$ vs SNL −1D. $n = 6$.

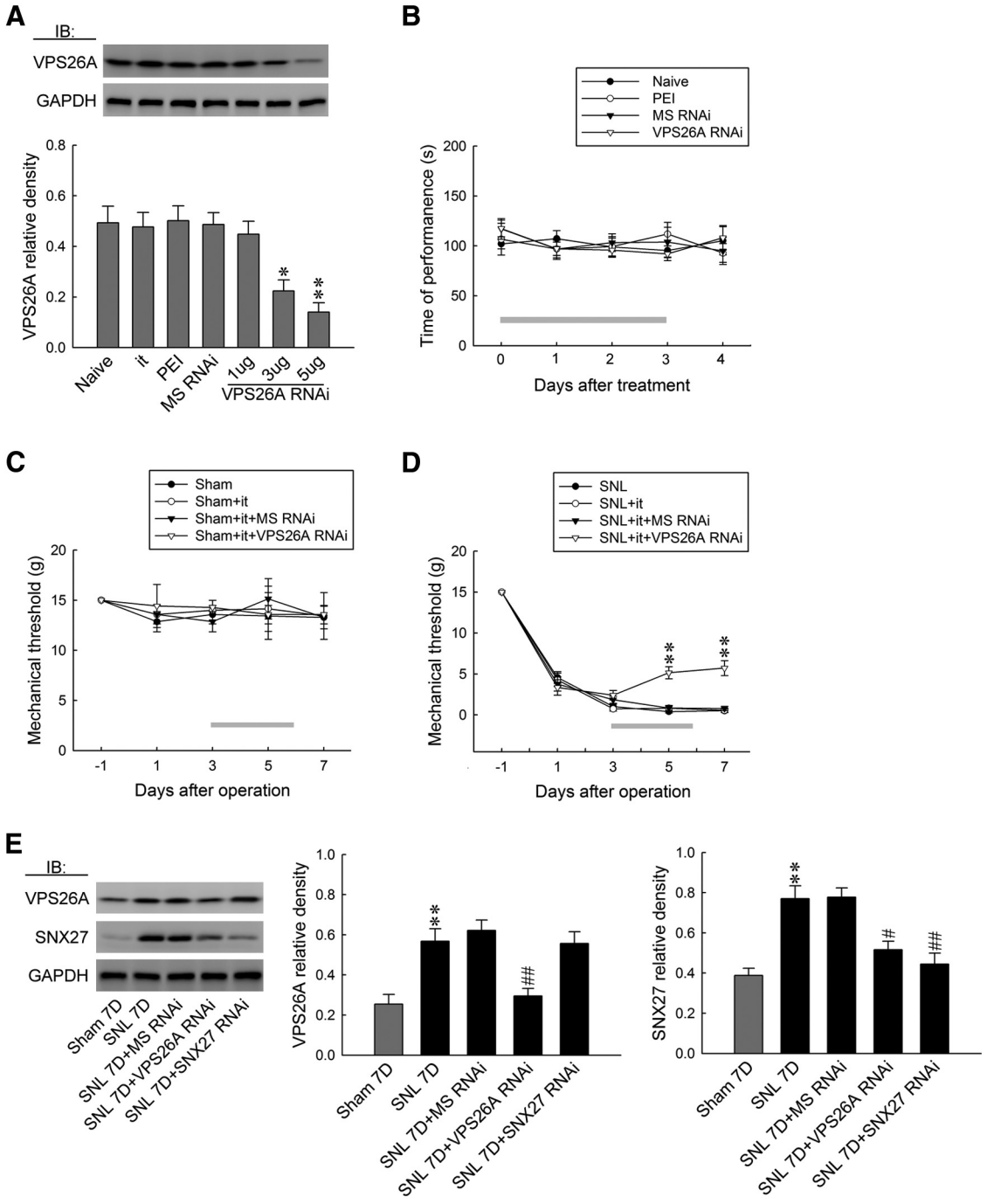

Figure 4. Focal knock-down of spinal VPS26A expression relieves SNL-associated allodynia and SNX27 expression. ***A***, Representative Western blot and statistical analyses (normalized to GAPDH) demonstrating intrathecal administration with VPS26A mRNA-targeting siRNA (VPS26A RNAi; 1, 3, and 5 μg; 10 μl), but not missense siRNA (MS RNAi, 5 μg, 10 μl), polyethylenimine (PEI, 10 μl), or intrathecal catheter implantation alone (it), dose-dependently decreased spinal VPS26A expression. One-way ANOVA, $F_{(6,35)} = 8.251$, $p < 0.001$, *post hoc* Tukey's tests. *$p < 0.05$, **$p < 0.01$ vs naive. $n = 6$. IB, Immunoblotting. ***B***, The application of VPS26A mRNA-targeting siRNA (VPS26A, 5 μg, 10 μl) resulted in no motor deficits in animals (Rotarod test). Two-way ANOVA with repeated measures over time, group ($F_{(3,24)} = 0.021$; $p = 0.995$), and time ($F_{(4,96)} = 0.992$; $p = 0.454$) and in the interaction of group by time ($F_{(12,96)} = 0.552$; $p = 0.907874$), *post hoc* Tukey's tests. $n = 7$. ***C***, ***D***, Although no effect on the withdrawal threshold of the sham-operated animal was observed, the focal knock-down of spinal VPS26A expression (SNL+it+VPS26A RNAi, 5 μg, 10 μl) ameliorated the SNL-decreased withdrawal threshold at days 5 and 7 after the operation (von Frey test). sham group, two-way ANOVA with repeated measures over time, group ($F_{(3,24)} = 0.125$; $p = 0.944$), and time ($F_{(4,96)} = 0.975$; $p = 0.424$) and in the interaction of group by time ($F_{(12,96)} = 0.174$; $p = 0.999$), *post hoc* Tukey's tests. $n = 7$. SNL group, two-way ANOVA with repeated measures over time, group ($F_{(3,24)} = 18.94$; $p < 0.001$) and time ($F_{(4,96)} = 503.0$; $p < 0.001$) and in the interaction of group by time ($F_{(12,96)} = 1.070$; $p < 0.001$), *post hoc* Tukey's tests. **$p < 0.01$ vs SNL. $n = 7$. ***E***, The SNL-increased abundance of VPS26A and SNX27 in dorsal horn samples (normalized to GAPDH) at day 7 after the operation was reduced through the focal knock-down of spinal VPS26A expression (SNL+it+VPS26A RNAi, 5 μg, 10 μl). Nevertheless, the administration with SNX27 mRNA-targeting siRNA (SNL 7D+SNX27 RNAi, 3 μg, 10 μl) attenuated SNL-enhanced spinal SNX27, but not VPS26A, expression. VPS26A, one-way ANOVA, $F_{(4,25)} = 10.84$, $p < 0.001$, *post hoc* Tukey's tests. SNX27, one-way ANOVA, $F_{(4,25)} = 13.72$, $p < 0.001$, *post hoc* Tukey's tests. **$p < 0.01$ vs sham 7D. #$p < 0.05$, ##$p < 0.01$ vs SNL7D. $n = 6$.

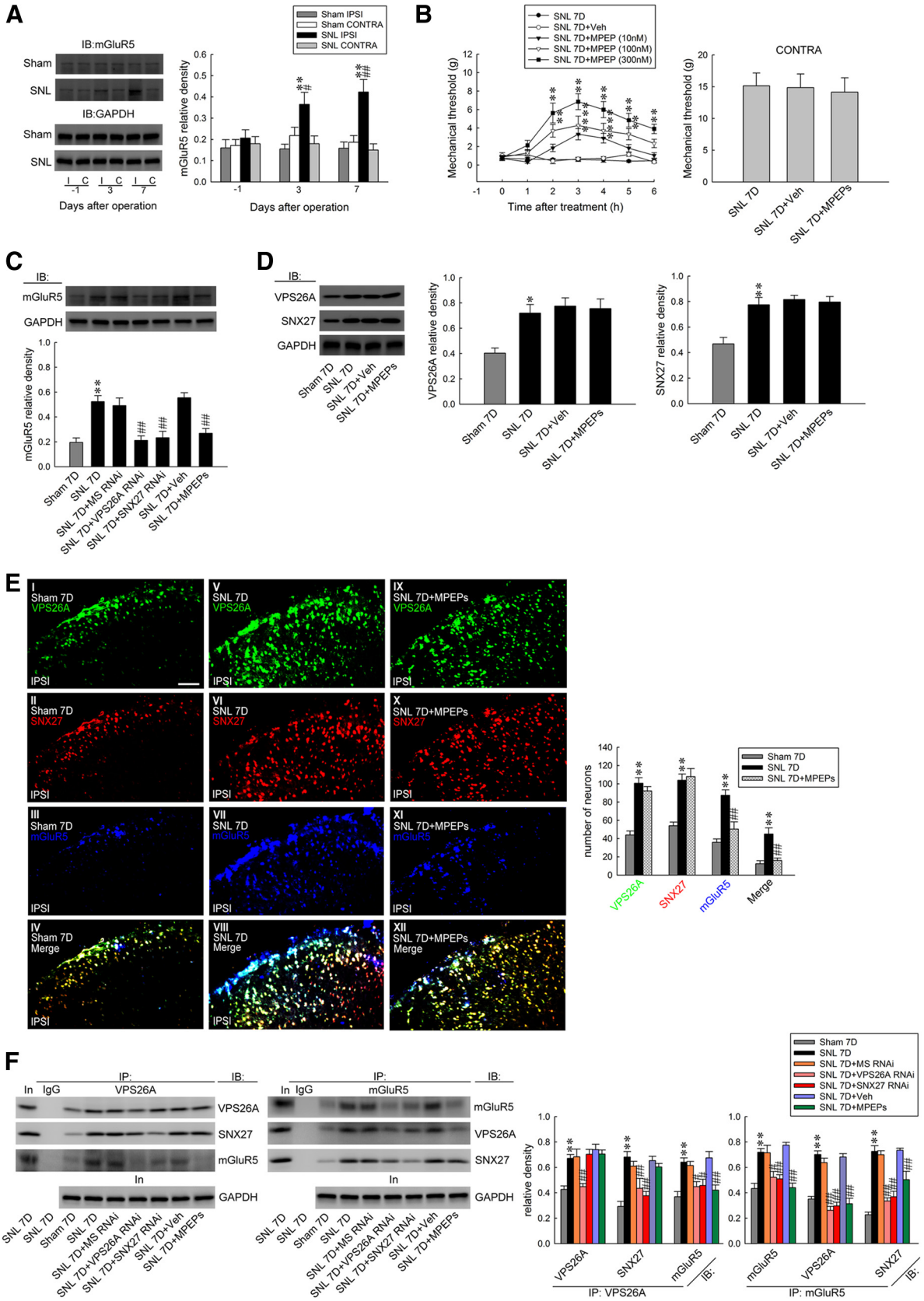

Figure 5. SNL induces mGluR5 expression and SNX27-VPS26A–mGluR5 interaction in the dorsal horn. ***A***, Representative Western blot and statistical analyses (normalized to GAPDH) revealing that SNL, but not the sham operation (sham), increased mGluR5 expression selectively in the ipsilateral (I and IPSI), but not the contralateral (C and CONTRA), dorsal horn at days 3 and 7 after the operation. Two-way ANOVA with repeated measures over time, group ($F_{(3,20)} = 12.53$; $p < 0.001$) and time ($F_{(2,40)} = 2.352$; $p = 0.108$) and in the interaction of group by time ($F_{(6,40)} = 2.378$; $p = 0.046$), *post hoc* Tukey's tests. $^{**}p < 0.01$ vs sham IPSI. $\#p < 0.05$, $\#\#p < 0.01$ vs SNL day −1; $n = 6$. IB, Immunoblotting. ***B***, On day 7 after the operation, the bolus injection of MPEP (SNL 7D+MPEP; 10, 100, and 300 nM; 10 μl, i.t.), but not the vehicle solution (SNL 7D+Veh, 10 μl, i.t.; von Frey test), increased the withdrawal threshold (*Figure legend continues.*)

horn neurons that underlie the development of behavioral allodynia.

These conclusions are based on the findings that neuropathic injury accompanied with behavioral allodynia time-dependently enhanced spinal SNX27 expression, which was immunohistologically coincident with the expression of a neuronal marker. Conversely, the focal knock-down of spinal SNX27 expression sufficiently attenuated SNL-induced behavioral allodynia, revealing a role for spinal SNX27 in neuropathic pain development. Moreover, SNL-induced allodynia was associated with enhanced VPS26A expression, VPS26A–SNX27 coprecipitation, and VPS26A-positive and VPS26A–SNX27 double-labeled immunoreactivity in the dorsal horn. Moreover, these effects were all sufficiently ameliorated through the focal knock-down of spinal VPS26A expression. Although the knock-down of SNX27 exhibited similar effects, it failed to affect SNL-enhanced VPS26A expression. Although the detailed mechanism of interactions between VPS26A and SNX27 remains unclear, these results suggest that spinal SNX27 acts as a downstream molecule of the retromer component VPS26A. Nevertheless, considering that the endosomal retromer complex rescues targeted proteins from the lysosomal degradation pathway and facilitates the recycling of these proteins to other cellular compartments (Gallon and Cullen, 2015), the possibility that the loss of VPS26A could enhance SNX27 degradation and thereby attenuate SNL-increased SNX27 abundance cannot be excluded. Moreover, although the administration of MPEP adequately ameliorated SNL-associated allodynia and mGluR5 expression and membrane insertion, it exhibited no effect on SNL-enhanced VPS26A or SNX27 expression and VPS26A–SNX27 coprecipitation or double labeling. In contrast, the knock-down of both VPS26A and SNX27 sufficiently ameliorated SNL-enhanced total and membrane-bound mGluR5 expression, mGluR5 coprecipitation, and colabeling with VPS26A and SNX27. Theses finding are consistent with a previous study indicating that a direct interaction between SNX27 and the retromer subunit VPS26 is necessary and sufficient to prevent the lysosomal entry of SNX27 cargo (Steinberg et al., 2013). These data not only provide supporting evidence for the contribution of the VPS26A–SNX27 complex in the endocytic recycling of membrane proteins, but to our knowledge, these results are the first to show an association between VPS26A–SNX27 complex-associated sorting machinery and the spinal plasticity underlying neuropathic pain, suggesting the potential physiological/pathological relevance of endocytic recycling in pain pathophysiology through modifications of mGluR5 recycling. Nevertheless, our data do not exclude the possibility that retromer signaling might modulate the function of spinal glutamatergic receptors other than mGluR5 to alter pain sensitivity because the SNX27–retromer complex was shown to facilitate GluA1 insertion into the plasma membrane of hippocampal neurons to modify memory-associated plasticity (Loo et al., 2014).

After pinching off from the plasma membrane, early endosomes initiate cargo sorting, principally into two distinct pathways: an endolysosomal degradation route that downregulates signaling receptors and a collection of distinct retrieval pathways that recycle cargo away from degradation (Cullen and Korswagen, 2012). Through cooperative coupling and functioning with associated proteins, including the SNX family, the retromer regulates endosomal sorting (Rojas et al., 2008; Burd and Cullen, 2014) and acts as a major hub required for endosomal recycling (Gallon and Cullen, 2015). In the present study, SNL induced VPS26A–SNX27 interactions accompanied by increases in the amounts of membrane-bound and total mGluR5 in dorsal horn neurons. The SNX27–retromer complex was found to be required for the homeostasis of the surface protein levels, as evidenced by the fact that, after LTP stimulation, SNX27 couples with and facilitates GluA1 insertion into the plasma membrane of hippocampal neurons. Conversely, SNX27 depletion reduces the abundance of surface-bound GluA1 (Loo et al., 2014). We therefore suggest that the increase in membrane-bound mGluR5 could be attributable to VPS26A–SNX27 complex-dependent endosome trafficking toward the plasma membrane. However, considering that a previous study showed that the abundance of glucose and metal transporters were reduced in the whole lysates of retromer- and SNX27-depleted HeLa cells, reflecting the enhanced lysosomal degradation of these proteins (Steinberg et al., 2013), we suggested that the enhanced mGluR5 abundance could result from reduced protein degradation. This proposal is based on the finding that SNL enhanced the abundance of both total and membrane-bound mGluR5 in the dorsal horn. Moreover, the focal knock-down of spinal VPS26A not only affected membrane-bound mGluR5, but also efficiently reduced the SNL-increased amount of total mGluR5, indicating that a loss of VPS26A results in mGluR5 degradation. This finding is consistent with a study that investigated rhodopsin recycling and degradation in *Drosophila* and demonstrated that the increased abundance of retromer-suppressed degradation and facilitated

←

(*Figure legend continued.*) of the ipsilateral hindpaw at hours 2–6 after the injection. Two-way ANOVA with repeated measures over time, group ($F_{(4,30)} = 69.00$; $p < 0.001$) and time ($F_{(6,180)} = 15.37$; $p < 0.001$) and in the interaction of group by time ($F_{(24,180)} = 4.150$; $p < 0.001$), *post hoc* Tukey's tests. $^{**}p < 0.01$ vs SNL 7D; $n = 7$. Nevertheless, neither treatment affected the contralateral hindpaw at 3 h after injection (SNL7D + MPEP 300 nM; 10 μl, i.t.; von Frey test). One-way ANOVA, $F_{(2,18)} = 0.057$, $p = 0.944$, *post hoc* Tukey's tests; $n = 7$. ***C***, The daily administration (day 3–6 after SNL) of VPS26A mRNA-targeting siRNA (SNL 7D + VPS26A RNAi, 5 μg, 10 μl, i.t.), SNX27 mRNA-targeting siRNA (SNL 7D + SNX27 RNAi, 3 μg, 10 μl, i.t.), and MPEP (SNL 7D + MPEPs; 300 nM; 10 μl, i.t.) ameliorated SNL-upregulated mGluR5 (normalized to GAPDH) expression at day 7 after the operation. One-way ANOVA, $F_{(6,35)} = 12.56$, $p < 0.001$, *post hoc* Tukey's tests. $^{**}p < 0.01$ vs sham 7D. $^{\#\#}p < 0.01$ vs SNL 7D. $n = 6$. ***D***, The daily administration of MPEPs (SNL 7D + MPEPs, 300 nM, 10 μl) did not affect the SNL-upregulated spinal VPS26A or SNX27 expression. VPS26A, one-way ANOVA, $F_{(3,20)} = 7.564$, $p = 0.001$, *post hoc* Tukey's tests. SNX27, one-way ANOVA, $F_{(4,25)} = 12.3$, $p < 0.001$, *post hoc* Tukey's tests. $^{*}p < 0.05$, $^{**}p < 0.01$ vs sham 7D; $n = 6$. ***E***, Image analyses demonstrate that SNL increased the VPS26A (green), SNX27 (red), mGluR5 (blue), and mGluR5/SNX27/VPS26A triple-labeled (white) immunofluorescence in the ipsilateral dorsal horn. The daily administration of MPEPs (SNL 7D + MPEPs, 300 nM, 10 μl) affects the SNL-upregulated spinal mGluR5 (blue) expression, but did not affect VPS26A (green) or SNX27 (red) expression. Paired two-tailed Student's *t* test, $^{**}p < 0.01$ vs sham 7D. $^{\#\#}p < 0.01$ vs SNL 7D; $n = 7$. Scale bar, 50 μm. Thickness, 50 μm. ***F***, At day 7 after the operation, the SNL-increased abundance of VPS26A-bound VPS26A, SNX27 and mGluR5, mGluR5-bound mGluR5, SNX27 and VPS26A were all attenuated through the daily administration of VPS26A mRNA-targeted antisense siRNA (SNL 7D + VPS26A RNAi; 5 μg, 10 μl). Application of SNX27 mRNA-specific antisense siRNA (SNL 7D + SNX27 RNAi; 3 μg, 10 μl) elicited similar effects, but did not reduce the amount of enhanced VPS26A-bound VPS26 in the precipitates. Application of MPEPs (SNL 7D + MPEPs, 300 nM, 10 μl) attenuated the SNL-increased abundance of VPS26A-bound mGluR5 and mGluR5-bound mGluR5, SNX27, and VPS26A, but did not affect the SNL-increased abundance of VPS26A-bound VPS26A and SNX27. The GAPDH abundance in the preprecipitated homogenates remained at a relatively constant level at these time points. No detectable immunoreactivity was observed in the control IgG-recognized precipitation. In, input control; IP, immunoprecipitation. VPS26A-bound VPS26A, one-way ANOVA, $F_{(6,35)} = 11.54$, $p < 0.001$; VPS26A-bound SNX27, one-way ANOVA, $F_{(6,35)} = 11.42$, $p < 0.001$; VPS26A-bound mGluR5, one-way ANOVA, $F_{(6,35)} = 8.778$, $p < 0.001$; mGluR5- bound mGluR5, one-way ANOVA, $F_{(6,35)} = 13.39$, $p < 0.001$; mGluR5-bound VPS26A, one-way ANOVA, $F_{(6,35)} = 40.42$, $p < 0.001$; mGluR5- bound SNX27, one-way ANOVA, $F_{(6,35)} = 29.83$, $p < 0.001$. All *post hoc* Tukey's tests, $^{**}p < 0.01$ vs sham 7D. $^{\#}p < 0.05$, $^{\#\#}p < 0.01$ vs SNL 7D. $n = 6$. No detectable immunoreactivity was observed in the control IgG precipitation. In, input control; IP, immunoprecipitation.

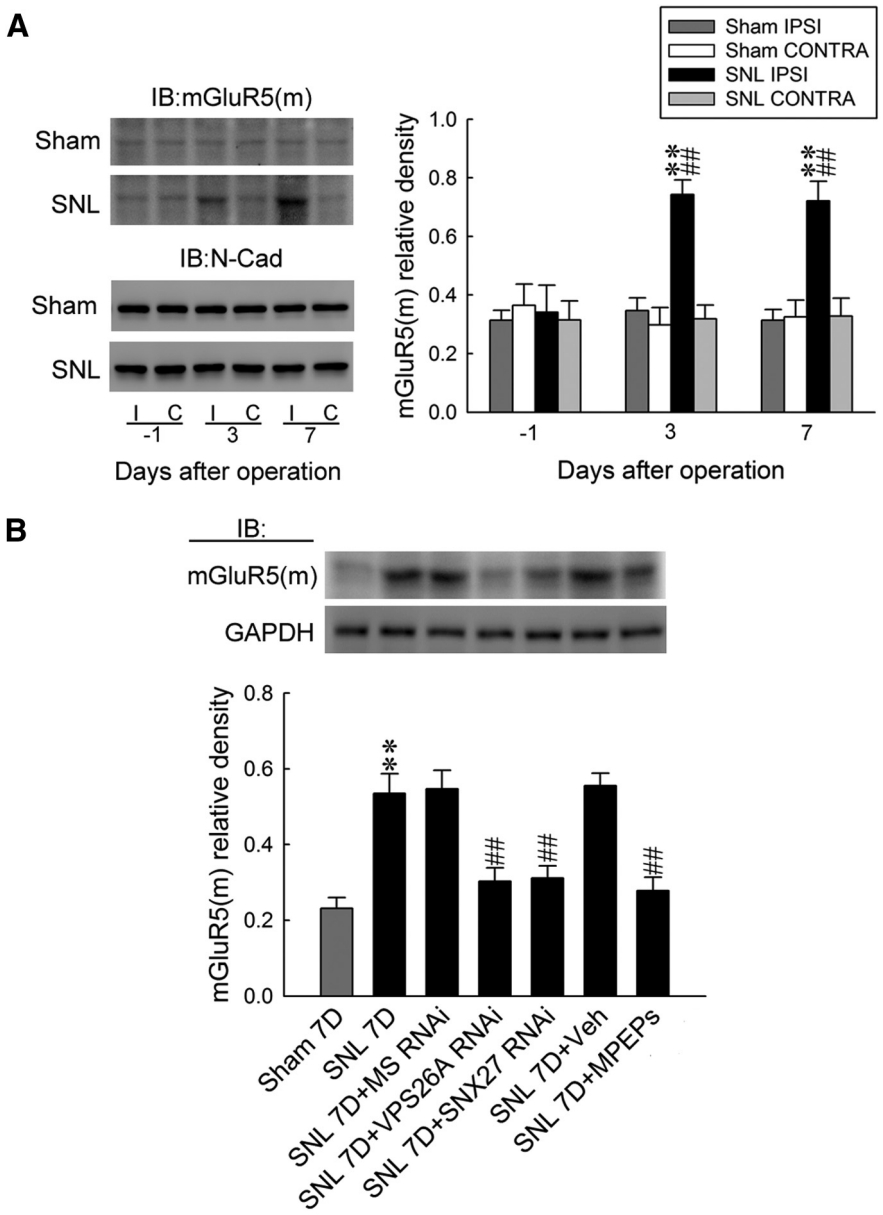

Figure 6. The VPS26A–SNX27 complex drives mGluR5 membrane trafficking to mediate neuropathic pain in the dorsal horn. ***A***, A representative Western blot and statistical analyses (normalized to *N*-Cad) showed that SNL, but not the sham operation (sham), increased the abundance of mGluR5(m) selectively in the ipsilateral (I and IPSI), but not contralateral (C and CONTRA), dorsal horn at days 3 and 7 after the operation. Statistical analyses included two-way ANOVA with repeated measures over time, group ($F_{(3,20)} = 28.47$; $p < 0.001$) and time ($F_{(2,40)} = 2.595$; $p = 0.087$) and in the interaction of group by time ($F_{(6,40)} = 3.281$; $p = 0.010$), *post hoc* Tukey's tests. $^{**}p < 0.01$ vs sham IPSI. $^{\#\#}p < 0.01$ vs SNL day −1, $n = 6$. IB, Immunoblotting. ***B***, Focal knock-down of spinal VPS26A and SNX27 expression using specific antisense siRNA (5 μg of SNL 7D + VPS26A RNAi and 3 μg of SNL 7D + SNX27 RNAi, 10 μl) and application of MPEPs (SNL 7D + MPEPs, 300 nM, 10 μl) all reversed the SNL-enhanced expression of membrane-bound mGluR5 on day 7 after the operation. One-way ANOVA, $F_{(6,77)} = 30.14$, $p < 0.001$, *post hoc* Tukey's tests. $^{**}p < 0.01$ vs sham 7D. $^{\#\#}p < 0.01$ vs SNL 7D. $n = 6$.

photoreceptor protein recycling; conversely, the lack of retromer resulted in the improper recycling and the degeneration of photoreceptor protein (Wang et al., 2014). Together, these data reveal that the SNL-enhanced VPS26A–SNX27 interaction is necessary and sufficient to regulate the endosomal recycling of mGluR5, which possibly impedes lysosomal degradation and promotes the membrane insertion of mGluR5 underlying the development of neuropathic pain. Nevertheless, Lunn et al. (2007) investigated the surface expression of the Kir3 potassium channel and demonstrated that SNX27 promotes endosomal movement, leading to the reduced surface expression of the Kir3 potassium channel in HEK293 cells. Although the mechanism underlying this discrepancy is not clear, these investigators did not identify the partner retromer of SNX27. Considering that the direct interaction of the SNX27 PDZ domain with the retromer subunit VPS26 is necessary and sufficient to prevent the lysosomal entry of SNX27 cargo (Steinberg et al., 2013), it is likely that, without coupling with the retromer, SNX27 could prompt cargo degradation. However, SNX27 exhibits a dissimilar effect that impedes degradation when associated with VPS26 because our data showed that SNL induces the spinal VPS26A–SNX27 interaction accompanied by the enhanced abundance of total mGluR5. The focal knock-down of spinal VPS26A, in which spinal SNX27 functions alone without the VPS26A partner, reduced the SNL-increased amount of total mGluR5; that is, it promoted mGluR5 degradation. However, the precise mechanism involved needs further investigation.

In the present study, administration of MPEP, an mGluR5 antagonist, decreased the amount of receptor expressed at the membrane. Although the mechanism underlying this MPEP-induced decrease in mGluR5 trafficking is not clear, mGluR5 receptors are demonstrated to be subject to an endogenous active cycle of phosphorylation and dephosphorylation (Orlando et al., 2002). In rat hippocampal neurons, phosphorylation of mGluR5 enhances mGluR5-Siah 1A binding, which is essential for Siah-1A's effects on mGluR5 trafficking (Ko et al., 2012). Therefore, we suggest that MPEP could antagonize mGluR5 phosphorylation and thereby reduce membrane-bound mGluR5 trafficking in dorsal horn neurons. Our proposal is supported by a study showing that drug-induced mGluR5 phosphorylation can be inhibited by MPEP (Ireland et al., 2004). Nevertheless, the elucidation of detailed mechanisms for these effects needs further investigation.

In conjunction with the retromer, the SNX family has been implicated in endosome recycling. For example, SNX-BAR-dependent (Wassmer et al., 2009) and SNX3-dependent (Harterink et al., 2011) export pathways contribute to cargo trafficking from endosomes to the *trans*-Golgi network. A recent study demonstrated that SNX27, a unique PDZ domain-containing SNX, transports cargo bearing the PDZ-binding motif from the endosome to the plasma membrane (Cullen and Korswagen, 2012). In the present study, the SNL-induced VPS26A–SNX27 complex interacts with and thereby recycles mGluR5 in dorsal horn neurons. Crystal structure analysis has revealed that the coupling of VPS26A to SNX27 increases the

affinity of the PDZ domain of SNX27 (Gallon et al., 2014) and, conversely, the uncoupling of VPS26A from SNX27 leads to the loss of cargo recycling from endosomes to the plasma membrane (Gallon and Cullen, 2015). Further, considering that mGluR5 is characterized by a PDZ motif-containing GPCR (Kitano et al., 2002) and SNX27 contributes to the subcellular recycling of the GPCR through PDZ-mediated protein–protein interactions (Bauch et al., 2014), we suggest that the SNL-induced SNX27-VPS26A complex interacts with mGluR5 via a PDZ-mediated interaction between SNX27 and mGluR5. This proposal is further supported by studies demonstrating retromer function in conjunction with associated proteins, including SNX (Gallon et al., 2015), and the VPS26A–SNX27 complex promotes recycling through PDZ-dependent cargo recognition (Temkin et al., 2011; Gallon et al., 2014). However, the detailed coupling mechanism between the VPS26A–SNX27 complex and mGluR5 warrants further investigation.

Notes

Supplemental material for this article is available at https://drive.google.com/file/d/0B1jrcoWKk82hU3ZiSUlfNXZ5ZVk/view. Shown are whole-blot images of VPS26A, SNX27, and mGluR5 probed by specific antibodies used in immunohistochemistry study. This material has not been peer reviewed.

References

Bauch C, Koliwer J, Buck F, Hönck HH, Kreienkamp HJ (2014) Subcellular sorting of the G-protein coupled mouse somatostatin receptor 5 by a network of PDZ-domain containing proteins. PLoS One 9:e88529. CrossRef Medline

Burd C, Cullen PJ (2014) Retromer: a master conductor of endosome sorting. Cold Spring Harb Perspect Biol 6: pii: a016774. CrossRef Medline

Collins BM, Skinner CF, Watson PJ, Seaman MN, Owen DJ (2005) Vps29 has a phosphoesterase fold that acts as a protein interaction scaffold for retromer assembly. Nat Struct Mol Biol 12:594–602. CrossRef Medline

Cullen PJ, Korswagen HC (2012) Sorting nexins provide diversity for retromer-dependent trafficking events. Nat Cell Biol 14:29–37. CrossRef Medline

Dunn HA, Ferguson SS (2015) PDZ protein regulation of GPCR trafficking and signaling pathways. Mol Pharmacol 88:624–639. CrossRef Medline

Ehlers MD (2000) Reinsertion or degradation of AMPA receptors determined by activity-dependent endocytic sorting. Neuron 28:511–525. CrossRef Medline

Galan A, Laird JM, Cervero F (2004) In vivo recruitment by painful stimuli of AMPA receptor subunits to the plasma membrane of spinal cord neurons. Pain 112:315–323. CrossRef Medline

Gallon M, Cullen PJ (2015) Retromer and sorting nexins in endosomal sorting. Biochem Soc Trans 43:33–47. CrossRef Medline

Gallon M, Clairfeuille T, Steinberg F, Mas C, Ghai R, Sessions RB, Teasdale RD, Collins BM, Cullen PJ (2014) A unique PDZ domain and arrestin-like fold interaction reveals mechanistic details of endocytic recycling by SNX27–retromer. Proc Natl Acad Sci U S A 111:E3604–E3613. CrossRef Medline

Hallett PJ, Collins TL, Standaert DG, Dunah AW (2008) Biochemical fractionation of brain tissue for studies of receptor distribution and trafficking. Curr Protoc Neurosci Chapter 1:Unit 1.16. CrossRef Medline

Harterink M, Port F, Lorenowicz MJ, McGough IJ, Silhankova M, Betist MC, van Weering JR, van Heesbeen RG, Middelkoop TC, Basler K, Cullen PJ, Korswagen HC (2011) A SNX3-dependent retromer pathway mediates retrograde transport of the Wnt sorting receptor Wntless and is required for Wnt secretion. Nat Cell Biol 13:914–923. CrossRef Medline

Hierro A, Rojas AL, Rojas R, Murthy N, Effantin G, Kajava AV, Steven AC, Bonifacino JS, Hurley JH (2007) Functional architecture of the retromer cargo-recognition complex. Nature 449:1063–1067. CrossRef Medline

Ireland DR, Guevremont D, Williams JM, Abraham WC (2004) Metabotropic glutamate receptor-mediated depression of the slow after hyperpolarization is gated by tyrosine phosphatases in hippocampal CA1 pyramidal neurons. J Neurophysiol 92:2811–2819. CrossRef Medline

Kim SH, Chung JM (1992) An experimental model for peripheral neuropathy produced by segmental spinal nerve ligation in the rat. Pain 50:355–363. CrossRef Medline

Kitano J, Kimura K, Yamazaki Y, Soda T, Shigemoto R, Nakajima Y, Nakanishi S (2002) Tamalin, a PDZ domain-containing protein, links a protein complex formation of group 1 metabotropic glutamate receptors and the guanine nucleotide exchange factor cytohesins. J Neurosci 22:1280–1289. Medline

Ko SJ, Isozaki K, Kim I, Lee JH, Cho HJ, Sohn SY, Oh SR, Park S, Kim DG, Kim CH, Roche KW (2012) PKC phosphorylation regulates mGluR5 trafficking by enhancing binding of Siah-1A. J Neurosci 32:16391–169401. CrossRef Medline

Larsson M, Broman J (2011) Synaptic plasticity and pain: role of ionotropic glutamate receptors. Neuroscientist 17:256–273. CrossRef Medline

Lee CY, Perez FM, Wang W, Guan X, Zhao X, Fisher JL, Guan Y, Sweitzer SM, Raja SN, Tao YX (2011) Dynamic temporal and spatial regulation ofmu opioid receptor expression in primary afferent neurons following spinal nerve injury. Eur J Pain 15:669–675. CrossRef Medline

Lin TB, Hsieh MC, Lai CY, Cheng JK, Chau YP, Ruan T, Chen GD, Peng HY (2015a) Modulation of nerve injury-induced HDAC4 cytoplasmic retention contributes to neuropathic pain in rats. Anesthesiology. In press. Medline

Lin TB, Lai CY, Hsieh MC, Jiang JL, Cheng JK, Chau YP, Ruan T, Chen GD, Peng HY (2015b) Neuropathic allodynia involves spinal neurexin-1β-dependent neuroligin-1/post-synaptic density-95/NR2B cascade in rats. Anesthesiology 123:909–926. CrossRef Medline

Loo LS, Tang N, Al-Haddawi M, Dawe GS, Hong W (2014) A role for sorting nexin 27 in AMPA receptor trafficking. Nat Commun 5:3176. Medline

Lunn ML, Nassirpour R, Arrabit C, Tan J, McLeod I, Arias CM, Sawchenko PE, Yates JR 3rd, Slesinger PA (2007) A unique sorting nexin regulates trafficking of potassium channels via a PDZ domain interaction. Nat Neurosci 10:1249–1259. CrossRef Medline

Luo C, Kuner T, Kuner R (2014) Synaptic plasticity in pathological pain Trends Neurosci 37:343–355.

Magalhaes AC, Dunn H, Ferguson SS (2012) Regulation of GPCR activity, trafficking and localization by GPCR-interacting proteins. Br J Pharmacol 165:1717–1736. CrossRef Medline

Martin S, Henley JM (2004) Activity-dependent endocytic sorting of kainate receptors to recycling or degradation pathways. EMBO J 23:4749–4759. CrossRef Medline

Orlando LR, Dunah AW, Standaert DG, Young AB (2002) Tyrosine phosphorylation of the metabotropic glutamate receptor mGluR5 in striatal neurons. Neuropharmacology 43:161–173. CrossRef Medline

Peng HY, Chen GD, Hsieh MC, Lai CY, Huang YP, Lin TB (2012) Spinal SGK1/GRASP-1/Rab4 is involved in complete Freund's adjuvant-induced inflammatory pain via regulating dorsal horn GluR1-containing AMPA receptor trafficking in rats. Pain 153:2380–2392. CrossRef Medline

Peng HY, Chen GD, Lai CY, Hsieh MC, Lin TB (2013) Spinal serum-inducible and glucocorticoid-inducible kinase 1 mediates neuropathic pain via kalirin and downstream PSD-95-dependent NR2B phosphorylation in rats. J Neurosci 33:5227–5240. CrossRef Medline

Pitcher MH, Ribeiro-da-Silva A, Coderre TJ (2007) Effects of inflammation on the ultrastructural localization of spinal cord dorsal horn group I metabotropic glutamate receptors. J Comp Neurol 505:412–423. CrossRef Medline

Rojas R, van Vlijmen T, Mardones GA, Prabhu Y, Rojas AL, Mohammed S, Heck AJ, Raposo G, van der Sluijs P, Bonifacino JS (2008) Regulation of retromer recruitment to endosomes by sequential action of Rab5 and Rab7. J Cell Biol 183:513–526. CrossRef Medline

Schäfers M, Svensson CI, Sommer C, Sorkin LS (2003) Tumor necrosis factor-a induces mechanical allodynia after spinal nerve ligation by activation of p38 MAPK in primary sensory neuron. J Neurosci 23:2517–2521. Medline

Steinberg F, Gallon M, Winfield M, Thomas EC, Bell AJ, Heesom KJ, Tavaré JM, Cullen PJ (2013) A global analysis of SNX27–retromer assembly

and cargo specificity reveals a function in glucose and metal ion transport. Nat Cell Biol 15:461–471. CrossRef Medline

Temkin P, Lauffer B, Jäger S, Cimermancic P, Krogan NJ, von Zastrow M (2011) SNX27 mediates retromer tubule entry and endosome-to-plasma membrane trafficking of signalling receptors. Nat Cell Biol 13:715–721. Medline

Trivedi RR, Bhattacharyya S (2012) Constitutive internalization and recycling of metabotropic glutamate receptor 5 (mGluR5). Biochem Biophys Res Commun 427:185–190. CrossRef Medline

Wang S, Tan KL, Agosto MA, Xiong B, Yamamoto S, Sandoval H, Jaiswal M, Bayat V, Zhang K, Charng WL, David G, Duraine L, Venkatachalam K, Wensel TG, Bellen HJ (2014) The retromer complex is required for rhodopsin recycling and its loss leads to photoreceptor degeneration. PLoS Biol 12:e1001847. CrossRef Medline

Wang W, Atianjoh F, Gauda EB, Yaster M, Li Y, Tao YX (2011) Increased expression of sodium channel subunit Nav1.1 in the injured dorsal root ganglion after peripheral nerve injury. Anat Rec (Hoboken) 294:1406–1411. CrossRef Medline

Wang X, Zhao Y, Zhang X, Badie H, Zhou Y, Mu Y, Loo LS, Cai L, Thompson RC, Yang B, Chen Y, Johnson PF, Wu C, Bu G, Mobley WC, Zhang D, Gage FH, Ranscht B, Zhang YW, Lipton SA, Hong W, Xu H (2013) Loss of sorting nexin 27 contributes to excitatory synaptic dysfunction by modulating glutamate receptor recycling in Down's syndrome. Nat Med 19:473–480. CrossRef Medline

Wassmer T, Attar N, Harterink M, van Weering JR, Traer CJ, Oakley J, Goud B, Stephens DJ, Verkade P, Korswagen HC, Cullen PJ (2009) The retromer coat complex coordinates endosomal sorting and dynein-mediated transport, with carrier recognition by the trans-Golgi network. Dev Cell 17:110–122. CrossRef Medline

Wen L, Tang FL, Hong Y, Luo SW, Wang CL, He W, Shen C, Jung JU, Xiong F, Lee DH, Zhang QG, Brann D, Kim TW, Yan R, Mei L, Xiong WC (2011) VPS35 haploinsufficiency increases Alzheimer's disease neuropathology. J Cell Biol 195:765–779. CrossRef Medline

Zimmermann M (1983) Ethical guidelines for investigations of experimental pain in conscious animals. Pain 16:109–110. CrossRef Medline